Laser Induced Shockwave as Delaminator of Composite Material for Ballistic Protection at High Strain Rate

Luminita-Cristina Alil, Michel Arrigoni, Marcel Istrate, Alexander Kravcov, Jérémy Le Pavic, and Gilles Tahan

Abstract Societal concerns on security push light weight armor for ballistic protection to remain a topic of interest. Ultra-High Molecular Weight Polyethylene composites (UHMWPE) have shown appreciable performances for ballistic protection, because of their ability to mitigate kinetic energy of projectiles by various mechanisms of dissipation and because of their lower density. Among dissipative mechanisms of interest, delamination is one of them. In order estimate the bond strength between two plies, the laser induced shock wave technique has been utilized on Tensylon® thin panels. Firstly, this paper introduces this technique and its capabilities with respect to the characterization of ballistic protections at very high strain rates (10^6 s^{-1}). Secondly, a set of experimental results is shown and interpreted to obtain the interply bond strength, through the spallation process. At last, experimental results are supported by a numerical model that is in the verge of being a predictive tool.

Keywords Tensylon® · UHMWPE · Ballistic protection · Laser shock wave · High strain rate

L.-C. Alil
Military Technical Academy, Bucharest, Romania

M. Arrigoni (✉) · J. Le Pavic · G. Tahan
ENSTA Bretagne, IRDL UMR CNRS n°6027, Brest, France
e-mail: michel.arrigoni@ensta-bretagne.fr

M. Istrate
SC STIMPEX SA, Bucharest, Romania

A. Kravcov
Faculty of Civil Eng, Czech Technical University, Praha, Czech Republic

2.1 Introduction

Societal concerns on security push light weight armor for ballistic protection to remain a topic of interest. Developing more efficient, light weight ballistic protective material is still a necessity for enlightening armored vehicle and personal protection; it will extend in a non-negligible way the autonomy and mobility. Composite materials open various possibilities in the field of ballistic armor due to their strong resistance and light weight. They have been extensively studied and thus they have been the object of numerous papers and even books [1, 2]. This association of fiber and matrix materials offers large combination of physical properties but has to be chosen in a relevant way. Cunniff presented a benchmarking of mechanical properties of the most utilized fibers in composite materials involved in ballistic protection [3].

With respect to these previous observations, we decided to focus on the delamination process that occurs during under shock and impact in composite material. In this paper we will present some of the results obtained by testing small UHMWPE laminate samples by the LASAT approach. Our motivations are developed in the following subsections of this introduction. Then, delamination experiments obtained by laser induced shock wave will be presented in paragraph 2. They are based on Photonic Doppler Velocimetry records of Tensylon samples subjected to laser induced shock waves. Paragraph 3 is dedicated to the loading induced by the laser induced shock wave. A numerical modeling of the delamination process is proposed in paragraph 4, by the use of the Finite Element Methods in explicit scheme. These results also include a discussion of key parameters of the model.

2.1.1 Motivation for Studying Tensylon®

By considering the most accessible fibers: glass, carbon, basalt, ultra-high-molecular-weight polyethylene (Tensylon®, Dyneema®, Spectra®), aramid (Kevlar®, Vectran®)... it is possible to use the Ashby method as a material selection process according to relevant criteria. In order to do so, the ratios ultimate stress over density and Young modulus over density were first considered for the mentioned fibers. The parameter introduced by Cunniff, $U*$, has been chosen for its evaluation with respect to the ratio of Young modulus over density. $U*$ is the product of fiber specific toughness and strain wave velocity and is expressed as (2.1):

$$U^* = \frac{\sigma\varepsilon}{2\rho}\sqrt{\frac{E}{\rho}} \tag{2.1}$$

Where σ and ε are respectively the ultimate tensile stress and strain of the considered fiber, E and ρ are respectively the Young modulus and the density of the fibers.

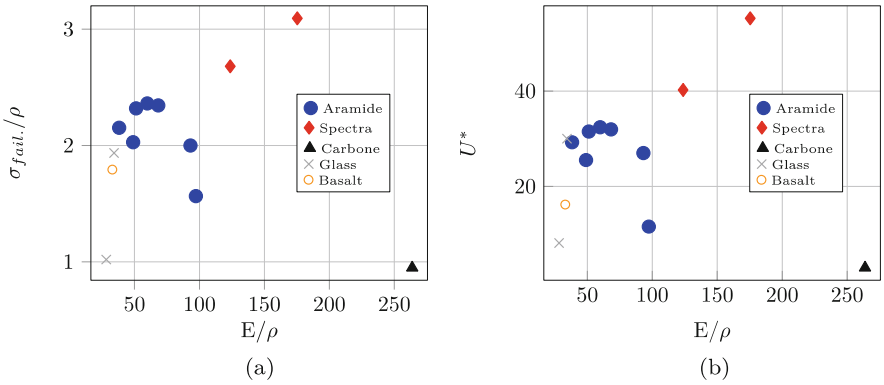

Fig. 2.1 Ashby method for material selection applied to fibers for composite used in ballistic protection. Left: Spectra (UHMWPE) exhibits the best compromise between stiffness, ultimate stress and density. Right: Spectra again shows the best score with respect of parameter $U*$ and the ratio E/ρ

Figure 2.1 shows both comparisons and highlights the fact that Spectra® - that belongs to the family of UHMWPE materials – is placed on the top right corner of the figure, meaning that this material is the most resistant, light and stiff in this material selection. Even though this Ashby approach appears to be basic, these preliminary observations strengthened our motivation to continue our research on UHMWPE. The choice of Tensylon® was brought by the partnership with STIMPEX S.A. Materials are described in Sect. 2.1.

2.1.2 Motivation to Focus on Delamination

Projectile penetration and perforation in composite plates are difficult topics to deal with so they involve various very brief phenomena that are occurring at the same time and are challenging to observe. Not only they strongly depend on the constitution of the target and the projectile itself, but also on the angle of incidence of the projectile, on its shape, on the boundary condition of the target. . . Energy dissipation mechanisms during the bullet penetration process can be the deformation and fragmentation of the bullet itself, but also friction, deformation, melting, fragmentation and delamination – or spallation – of the target and its constituents. Nevertheless, Zhang et al. [4] has proposed a relevant description of the phenomenon in UHMWPE (see Fig. 2.2a). They suggested a three stages description: at the first stage, the projectile interacts and penetrates the first plies of the target, by shear plugging, without causing large deformation. In the second stage, the projectile is deformed and expands in the cavity left within the composite. In the third stage, a spall appears close to the free surface and a crack is propagated in a rupture plane

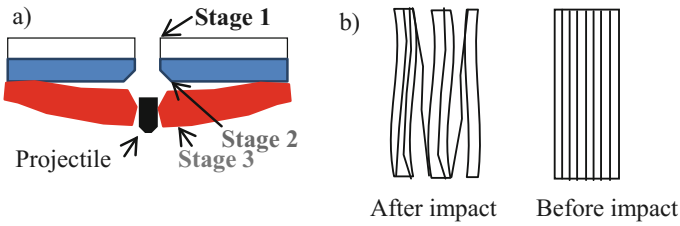

Fig. 2.2 Left: 3 stages damage mechanism proposed by Zhang on UHMWPE [4]. Right: accordion like multi-delamination in UHMWPE Dyneema® observed by Lässig after plate impact [5]

parallel to the free surface. Layers constituting the free surface are severely deformed and create a bulge. The projectile, at last, flies out of the target. Authors carried out experiments of shooting conically cylindrical steel projectile of 7.82 mm in diameter and 7.97 g in mass at about 700 m/s onto unidirectional plies of UHMWPE pressed in [0°;90°] of various thicknesses, respectively 8.4 mm, 16.92 mm and 25.24 mm. They observed the thicker the sample, the more represented bulge and delamination. For the thicker sample, they estimated stage 3 to be responsible of 72% of the bullet kinetic energy absorption. Delamination has also been reported by Lässig after plate impact experiments on UHMWPE recorded at high speed frames [5] (see Fig. 2.2b).

Under these considerations, this article proposes to assess the delamination of UHMWPE Tensylon®. Plies are manufactured by DuPont®, USA and pressed at STIMPEX S.A. in Romania in a [0°; 90°] stack sequence.

2.1.3 Some Considerations about Ballistic Impacts

Experimental measurements of the pressure induced by a ballistic impact on a target remain difficult to find in the open scientific literature. Some explanations for this limitation are, among others:

The mechanical failure of the sensors during the impact (damage, perforation),
The difficulty of implementing the sensors at the exact location of the impact,
The active surface of the sensor in front of the punctuality of the impact,
The geometrical singularity of bullets,
The diversity of projectiles.

It is therefore difficult to estimate this impact pressure other than by analytical simplifications or by the use of numerical simulation.

Hopkinson [6], on basic assumptions, proposed an analysis relying on the impact of a Mark VI steel bullet, 7.7 mm × 31.75 mm caliber, impacting a steel target at 610 m/s. He managed to estimate the duration of the peak pressure at about 52 µs for a maximum force of 19,300 Kg force distributed over the average section of the ball, that is to say more than 3 GPa.

Table 2.1 Estimated maximum impact pressure and duration of a ballistic impact

Target	$r_{projectile} = 3.5$ mm	$V_0 = 800$ m/s	$V_0 = 400$ m/s
PE	τ_p (μs) with (2)	8.0	12.6
	P_{max} (GPa)	2.5	1.0

Hutchings [7], based on a simple phenomenological analysis relying on the impact of a steel spherical, rigid projectile on a metal target, proposes to estimate the loading time τ_p during a ballistic impact by relation (2.2):

$$\tau_p = \pi.\omega_p \tag{2.2}$$

where ω_p is the pulsation in a plastic regime, expressed by the expression (2.3):

$$\omega_p = \frac{1}{r}\sqrt{\frac{3P_{max}}{2\rho}} \tag{2.3}$$

with r the sphere radius, P_{max} the "indentation pressure" at impact and ρ the density of the projectile.

The indentation pressure can be assimilated to the impact pressure that is determined via the shock polar technique (1D) as a first approximation. This latter approach carried out on a steel projectile impacting a bulk polyethylene target (PE) gives a maximum impact pressure of approximately $P_{max} = 2.5$ GPa for a projectile of incident velocity $V_0 = 800$ m / s (representative performance of an assault rifle). This pressure decreases to 1 GPa if the impact velocity is reduced by half (case of handguns). Applying formulas (2.2) and (2.3), the loading time induced by the ballistic impact can be estimated. These results are collated in Table 2.1 for a projectile radius of 3.5 mm (intermediate between 7.62 mm and 5.56 mm caliber).

These data were compared with numerical simulation results from Tham [8] who have reviewed various projectiles on a variety of Kevlar® composite helmet solutions. They announced pressure peaks close to 8 GPa for Fragment Surrogate Projectile (FSP) striking at 680 m/s with a diameter of 5.385 mm × 6.35 mm with an interaction duration of about 2 μs.

2.1.4 Motivation to Use Laser Induced Shock Waves

Laser induced shock waves are produced when focusing a short-duration and high-energy pulsed laser beam (~ ns, ~ J) on a small solid surface. In such a situation, the density of power, defined by relation (2.4) reaches a value of some GW/cm^2:

$$\phi = E_{max}/(\tau.S) \tag{2.4}$$

where ϕ is the density of power, E_{max} the maximum energy delivered by the laser source during duration τ and S the surface irradiated by the laser beam.

Under these conditions, the solid matter is quasi instantaneously dissociated into plasma and start its sudden expansion, in the same way as detonation products of high explosive do. The laser-matter interaction induces a shock wave in the irradiated material. The maximal pressure of this shock wave is called the ablation pressure and depends on the laser source characteristics and the irradiated material.

Laser induced shock wave have been extensively studied last decades for their involvement in the Laser Shot Peening (LSP) for material processing [9]. In LSP, the laser-matter interaction takes place in a water environment, that confines the plasma expansion, leading to stronger ablation pressures and longer pulse durations. Berthe [11] has proposed an analytical expression (2.5) that gives the maximum ablation pressure in function of the density of power involved in the laser irradiation (see Fig. 2.4):

$$\mathrm{P(kBar)} = 0.1\sqrt{\frac{\alpha}{\alpha+3}}\sqrt{Z(g.cm^{-2}.s^{-1})}\sqrt{I_0(GW/cm^2)} \tag{2.5}$$

Where P is the ablation pressure, I_0 is the incident density of power, α is a coefficient of laser-matter interaction that depends on the laser source, adjusted from experiments and Z is given by relation (2.6):

$$\frac{2}{Z} = \frac{1}{Z_{eau}} + \frac{1}{Z_{cible}} \text{ with } Z_i = \rho_{0i} C_{0i} \tag{2.6}$$

Where C_{0i} and ρ_{0i} are respectively the sound velocity and the density of the material $_i$.

Figures 2.3 and 2.4 show actually that it is possible, with a laser source, to generate the same pressure as the one undergone by the target during a ballistic impact. However, the pulse duration is more than 100 times shorter in the case of a classical laser induced shock wave. In the case of homogeneous materials, it could be possible to apply similitude laws that could result in a reduction of the target thickness, but in the case of composite or granular material, the thickness would become the order of magnitude of the grain or fiber size, what will induce predominant structural effects.

Laser induced shock waves have also been the object of the development of the LAser Shock Adhesion Test LASAT that permits the debonding of layered materials by inducing spallation inside the sample [10]. This technique has been successfully utilized for generating an interply debonding with composite materials [12]. This debonding is a consequence of the rarefaction of the shock wave at the free surface.

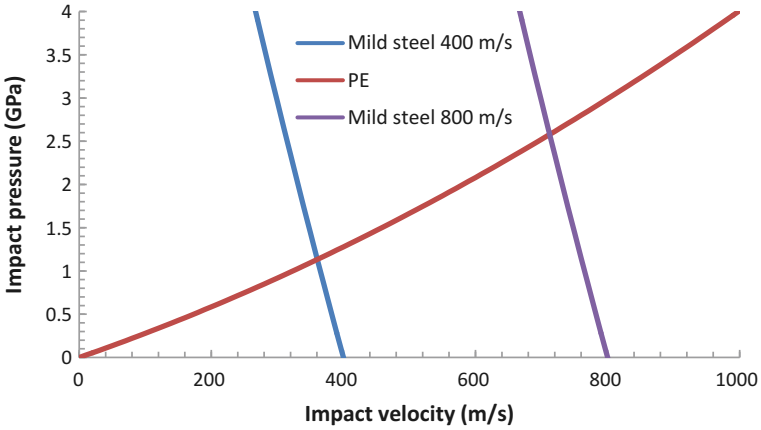

Fig. 2.3 Shock polar diagram for a 1D impact of a steel projectile on a PE target

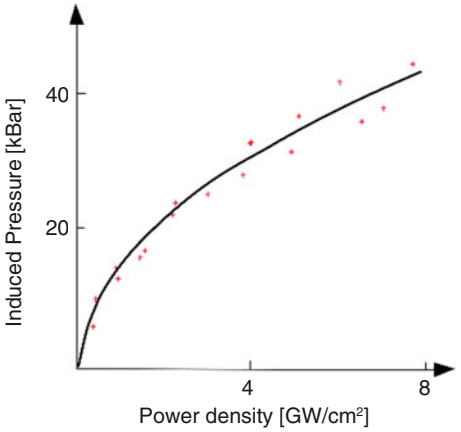

Fig. 2.4 Ablation pressure during laser-matter interaction in water environment [11]

The resultant rarefaction wave interacts with the rarefaction wave of the unloading that creates a tensile stress. The wave propagation is represented in a Lagrange diagram (see Fig. 2.5.)

Laser shock waves and ballistic impacts can access the same level of pressure but not the same duration. As it was explained, the sample thickness cannot be diminished by a factor 100. Nevertheless, the shortness of the laser impulse makes possible the delamination process shown on Fig. 2.5, that support our idea of focusing on delamination.

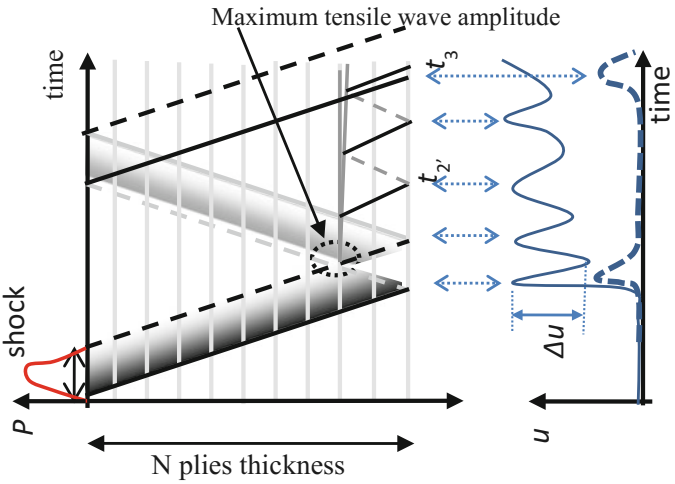

Fig. 2.5 Spallation process in composite material by laser induced shock wave

2.2 Experiments

2.2.1 Samples Description

Tensylon® HSBD 30A precursor tapes are bi-layered and bidirectional tapes. Each layer is composed of unidirectional UHMWPE fibres (UD) with about 20% of adhesive matrix [2]. These precursor tapes were submitted to quasi static mechanical tests for observing their mechanical response with respect to the strain rate in quasi-static regime in a tensile machine [13]. They were also stacked in [0°-90°] and pressed at 15.2 MPa and cured at 120 °C, in four stages for forming a plate (Table 2.2). From this 22 mm thick plate, cylinders of 20 mm diameter were cut and submitted to Hopkinson bars with strain rates up to 360 s^{-1} in order to determine a constitutive law [14]. They used an inverse approach by performing numerical simulation in order to fit experimental results. They determined a relatively precise parameter calibration for a simple plastic kinematic material model, by using two approaches: meso model and macro model. They suggested a Young Modulus of 3000 MPa, Poisson ratio of 0.47, Yield stress of 60 MPa and Tangential modulus of 500 MPa. In [15], a full UHMWPE plate of 500∗500 mm was impacted with 7.62∗39 mm FMJ with lead core bullet at 700 m/s. Micro and macroscopic observations are given and among dissipative mechanisms identified, multi-delamination is observed. An attempt to a numerical modelling is given in [16] including earlier advances performed by this research team. They implemented an approximate adhesive model and could obtain fairly satisfying results that allow them to evaluate strain rate at $1.16.10^5$ s^{-1}. They could estimate the stopping time of the projectile to be between 8 and 14 μs depending on the modelling assumptions, with an impact

Table 2.2 Pressing stages for Tensylon® hard ballistic plates

Stage	Pressure [MPa]	Temp. [°C]	Duration [min]
1	4.1	60	15
2	8.1	100	45
3	15.2	120	90
Cooling		120- > 30	Overnight

pressure of 2 GPa before elements deletion, in fairly agreement with data projected in Table 2.1. In the simulation, they highlight that having an adhesive model between plies changes significantly the results in term of interaction time between the bullet and the target and also in term of pressure at impact. It is thus a need to model delamination with a more accurate data, especially by knowing the interply bond strength. Another experimental campaign was then conducted to obtain the delamination threshold at very high strain rate by using the laser induced shock wave technique as a delaminator [17].

Samples were prepared from a Tensylon® plate that was water jet cut in small samples (10 × 20 mm), having thicknesses of and 2.45 mm (40 layers) and 1.15 mm (20 layers). During first attempts, it has been found that UHMWPE is transparent to the 1064 nm wavelength in such a way that the laser-matter interaction was not reproducible and not strong enough. To remediate this, a 15 μm layer of Aluminium foil was stuck on the irradiated face of the sample, with a cyanoacrylate Super Glue®. The thickness of this glue layer was measured by differences and estimated to be between 8 and 10 μm. It is assumed that the shock impedance of the glue matches with the one of the UHMWPE, in such a way that the shock propagation is not perturbed by this artefact.

2.2.2 Experimental Setup

The High energy laser source available at ENSTA Bretagne is a pulsed Nd-YAG laser, model Quanta-Ray Pro 350, manufactured by Spectra-Physics®. The maximum energy it can provide is $E_{max} = 3.8$ J max, in its fundamental wavelength $\lambda = 1064$ nm with a quasi-Gaussian pulse of duration at full width at half maximum $\tau = 9.2$ ns measured by ultra-fast photodiode. The laser beam diameter at the output is 13 mm with a small divergence. This beam is focused on the sample by a convergent lens to get a focal spot of area S on the sample. The focal sport was 3 mm of diameter. On the other side of the sample, at the center of the projected focal spot, a sensing laser of a Photonic Doppler Velocimetry (PDV) system – also called Heterodyne Velocimetry (HV) - manufactured by IDIL® is measuring the free surface velocity during the shock experiment. The wavelength of the PDV laser is 1550 μm. A layout of the experimental setup is shown on Fig. 2.6.

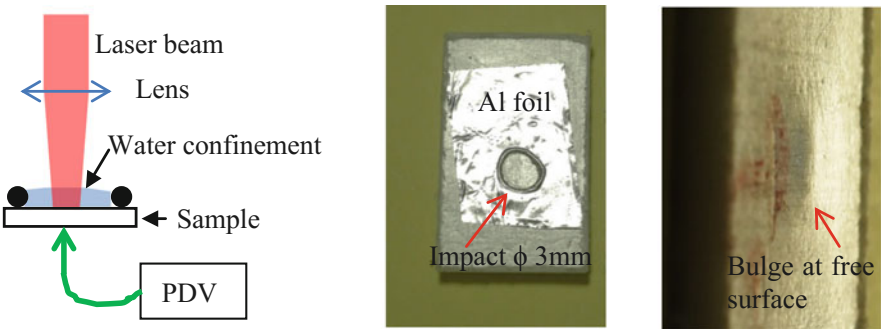

Fig. 2.6 Left: Experimental setup of laser shock wave on UHMWPE. Center: trace of impact resulting from the laser-matter interaction. Right: visible bulge at the free surface

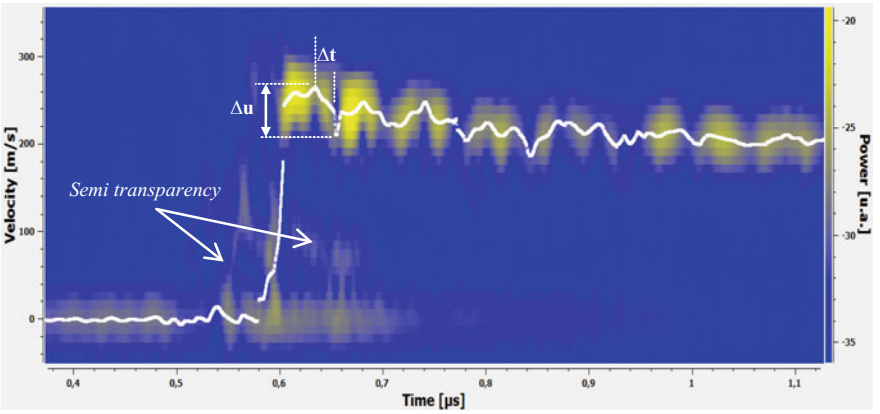

Fig. 2.7 Spectrogram of the PDV signal obtained for sample T-9 of 1.15 mm of thickness, irradiated at 1.8 GW/cm^2. In white, velocity data extraction by Cafeine software

2.2.3 Experimental Results

Experimental results are mainly from the PDV signals analysis and may be completed by macroscopic observations. They are exhibited and discussed in [17]. As an example, a PDV signal is shown in Fig. 2.7. The main shock wave reaches the rear face around 0.6 µs and the maximal velocity rises up to 267 m/s. Before and after this rising front, some parasites are visible because of the transparency of the UHMWPE to the PDV laser. The maximum free-surface velocity, noted u_0, and the first free-surface velocity valley, u_m, can be read on the PDV spectrogram after speed extraction with Cafeine software [18], giving the white marks on Fig. 2.7. The dynamic tensile strength σ_{spall} can be deduced from linear approximation (2.7)

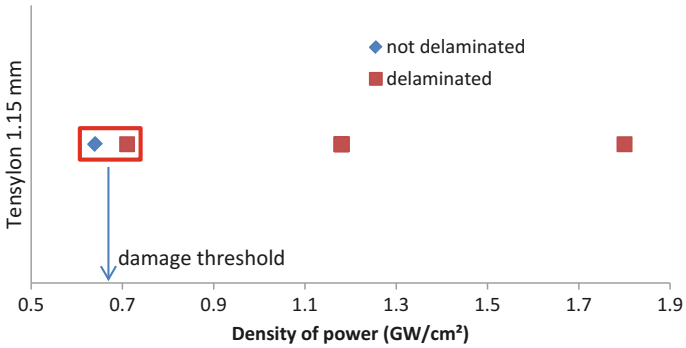

Fig. 2.8 Damage threshold in density of power for 1.15 mm thick Tensylon®

proposed by Novikov for isotropic material [19] but that has been extended to our composite materials, as considered in previous studies [12]:

$$\sigma_{spall} = \frac{1}{2}\rho_0 C_0 \Delta u \tag{2.7}$$

where $\Delta u = u_0 - u_m$ is the so-called "velocity pullback". From this velocity pull-back it is also possible to estimate the strain rate with the relation (2.8):

$$\dot{\varepsilon} = \frac{1}{2C_0}\frac{\Delta u}{\Delta t} \tag{2.8}$$

As an example of accessible values for shot T-9 presented (Fig. 2.7), $\sigma_{spall} = 45.8 \pm 5$ MPa with $\rho_0 = 0.94$ g/cm^3 and $C_0 = 1798$ m/s and the referred strain rate reached 2.2×10^6 s^{-1}. This strain rate acting between two plies and is thus related to the delamination process. A summary of the results obtained on the set of Tensylon® samples is given on Fig. 2.8. The damage threshold in density of power has been found between 0.64 and 0.71 GW/cm^2 for 1.15 mm thick Tensylon®.

2.3 Laser Shock Wave Characterisation

In order to perform a numerical modelling of these experiments, it is necessary to first model the laser shock loading, as it is the main input parameter. This section gives spatial and temporal profiles of the corresponding loading generated by the laser matter interaction.

In order to characterize the pressure profile induced by the laser-matter interaction of the ENSTA Bretagne pulsed laser, shots on 1 mm and 2 mm thick aluminum plates were performed with PDV records of the free surface velocity with the same experimental setup presented in paragraph 2.2. This procedure is detailed in [20].

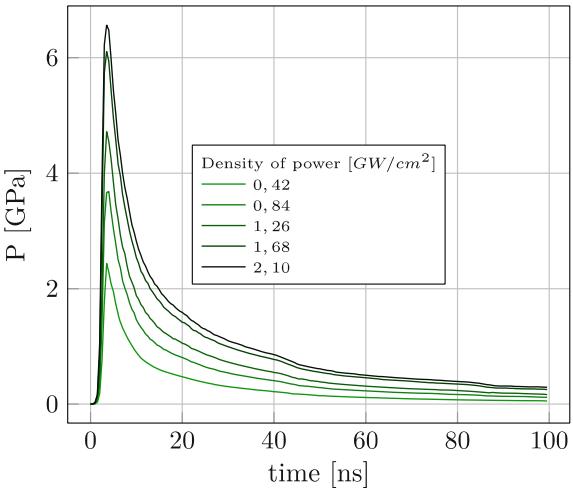

Fig. 2.9 Temporal profile of the pressure loading caused by the laser-material interaction with the ENSTA Bretagne pulsed laser characteristics (9.2 ns, 1064 nm) in confined water regime with a 4 mm focal spot

Table 2.3 Numerical values of the relation between energy density and the pressure generated by the ENSTA Bretagne laser

Parameter	*a*	*b*	*n*
Values	0.02922	−0.5867	0.3722

These tests provide a basis of comparison for validating the laser-matter interaction models. Figure 2.8 illustrates the pressure profiles as a function of the maximum energy fraction at the output of the laser, in water confined mode.

The energy distribution within the focal spot was estimated from a scan analysis of a laser shot on a photo paper. The average intensity obtained reveals a "flat-top" profile as delineated in Fig. 2.9 (red profile).

According to previous works, the pressure generated by laser shot could be calculated by using Eq. (9)

$$\mathrm{P(r)} = \mathrm{a}\phi^{\mathrm{n}} + \mathrm{b} \tag{2.9}$$

With P in GPa, ϕ in J/m^2, other parameters are listed in Table 2.1. This methodology is purely empirical. The fitted parameters are only available the presented laser and the laser pulse applied in this study. The pressure was calculated by using the ESTHER code as described as in [21] (Table 2.3).

As illustrated in Fig. 2.2, the energy density presents an evolution according to the radius of the laser spot. This energy density is estimated along the radius length. The associated pressure is calculated according the Eq. (2.9) previously presented. The procedure to obtain the equivalent pressure profile generated by the laser is delineated in Fig. 2.3.

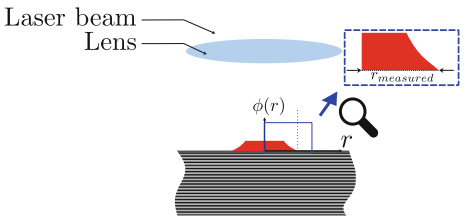

Fig. 2.10 Schematic illustration of the energy distribution in laser matter interaction

This procedure is detailed in the literature in [22]. This spatial distribution is normalized between [0;1]. The temporal profile is estimated from Fig. 2.1 and the pressure value is normalized between [0;1] also. The maximum value is given by the procedure illustrated in Fig. 2.10.

2.4 Numerical Modelling

The section describes the numerical modelling performed with Abaqus explicit of the experiment previously presented in paragraph 2. The sample is a Tensylon® UHMWPE composite made of 20 layers with a thickness of $1.15.10^{-3}$ m. An aluminum foil is located at the top of the sample for creating the laser-matter interaction, as explained in Sect. 2.2.

In order to simplify the modelling, strong assumptions are made. The laser shock wave is assumed to be generated on a line pattern whereas it is a quasi-circular spot. This approximation will not restitute the correct wave propagation in a long duration time but allows modelling in a 3D slice - 1D like geometry, since Abaqus cannot deal with cohesive contacts in 1D or 2D. In order to get an observation time shorter that the duration of a back and forth in the whole target, edge effects are not considered. The thin 3D slice ($5.0.10^{-5}$ m) of the structure is considered as illustrated in the Figs. 2.11 and 2.12. An 8-node reduced integration element type (C3D8R in Abaqus) is used to simulate the composite ply and the aluminum foil. Only one element is used in the model width, the influence on the mesh size will be discussed.

The UHMWPE Tensylon® is simulated with an elastoplastic behavior as described in Sect. 2.1. The numerical model considers the aluminum foil by using a Johnson-Cook behavior law [23].

Material characteristics of the constitutive law and Equation of State (EOS) are summarized in Table 2.4. They were taken from [5, 14]. The Abaqus module can only consider shear modulus when the Equation Of State (EOS) parameters is implemented in the model. The presented results considered a shear modulus $G = 850{,}0$ MPa to fit with the experimental data. The interfacial layer is simulated by contact cohesive interactions. Parameters used to simulate the interfacial stiffness between ply are presented in Table 2.5, where the interfacial is denoted K_i and the interfacial strength σ_i, with $i = n$, t_1 ot t_2 which correspond respectively the normal

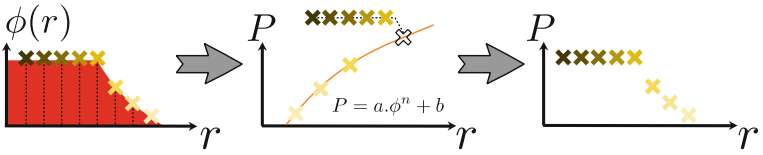

Fig. 2.11 Procedure used to estimate the equivalent spatial pressure generated by laser shock

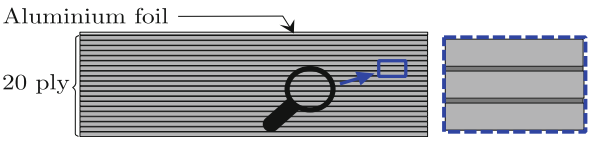

Fig. 2.12 Viewcut of the specimen used for laser shock wave tests

Table 2.4 Material data set for numerical simulation of Tensylon [14]. Missing data are completed by Dyneema parameters given by Lässig [5]

Parameters	Symbols	Values	Units
Mechanical properties [14]			
Density	ρ	960	Kg/m^3
Young modulus	E	2.5	MPa
Poisson's ratio	ν	0.47	/
Shear modulus	G	850	MPa
Elastic limit	σ^y	60	MPa
Tangential modulus	E^{tan}	500	MPa
Equation of state (EOS) [5]			
Grüneisen coefficient	Γ	1.6	/
Bulk sound velocity	C_0	1860	m/s
Shock EOS coefficient	S	1.8	/

Table 2.5 Interfacial parameter used for the cohesive contact

Parameters	Symbols	Values	Units
Stiffness of the interface			
Normal direction	K_n	$2.5.10^{+11}$	N
Tangential direction 1	K_{t1}	$2.5.10^{+11}$	N
Tangential direction 2	K_{t2}	$2.5.10^{+11}$	N
Initiation			
Normal direction	σ_n	45.0	MPa
Tangential direction 1	σ_{t1}	45.0	MPa
Tangential direction 2	σ_{t2}	45.0	MPa
Evolution			
Normal direction	G_I^c	3.0	N/m
Tangential direction 1	G_{II}^c	3.0	N/m
Tangential direction 2	G_{III}^c	3.0	N/m

and tangential directions. The fracture toughness is denoted G_i^c with $i = I$ (traction-compression), *II* (shear) or *III* (torsion) according to the crack opening mode.

Only, the shear modulus of the UHMWPE is considered in the Abaqus model. The equation of state (EOS) based on Mie-Grüneisen work is used. The velocity (normal to the surface) is averaged on a segment of 0.25 mm as illustrated (in red in Fig. 2.13) in order to represent alignment uncertainties (± 0.5 mm) and the spot size of the PDV probe (0.1 mm).

Under the laser-matter interaction, the pressure arises and causes a strong deformation of the Tensylon. Waves propagate in the sample thickness and create multi delamination that is represented in Fig. 2.14. It was not possible to confirm by cutting and performing optical observation in the recovered sample because of the fiber toughness that make the material hard to cut and polish.

The numerical velocity presented the average values of nodes illustrated Fig. 2.14. The mesh size has a strong influence on the FEA results as visible in Fig. 2.15. According to these results a mesh size of $5.0.10^{-6}$ m gives acceptable results and will be utilized in the following.

The comparison between the velocity measured experimentally and the one obtained from the numerical model is presented in Fig. 2.16. The FEA results present the average velocity of the nodes selected on a length of 0.25 mm as explained in Fig. 2.14. They show a good agreement since the standard deviation is lower than 3.5 m/s.

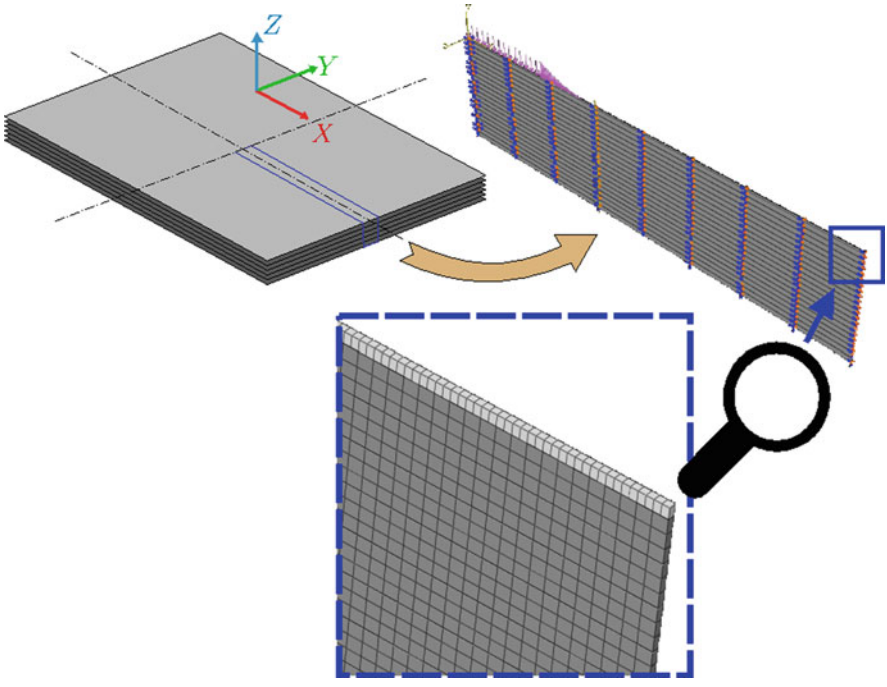

Fig. 2.13 Illustration of the model used to simulate laser wave experiments

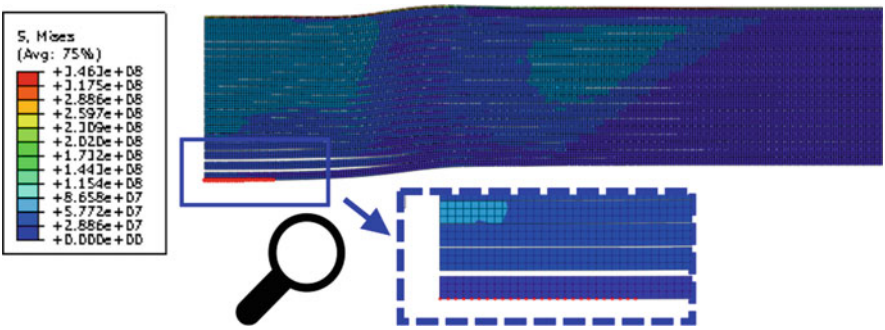

Fig. 2.14 Extraction of the velocity at nodes represented in red

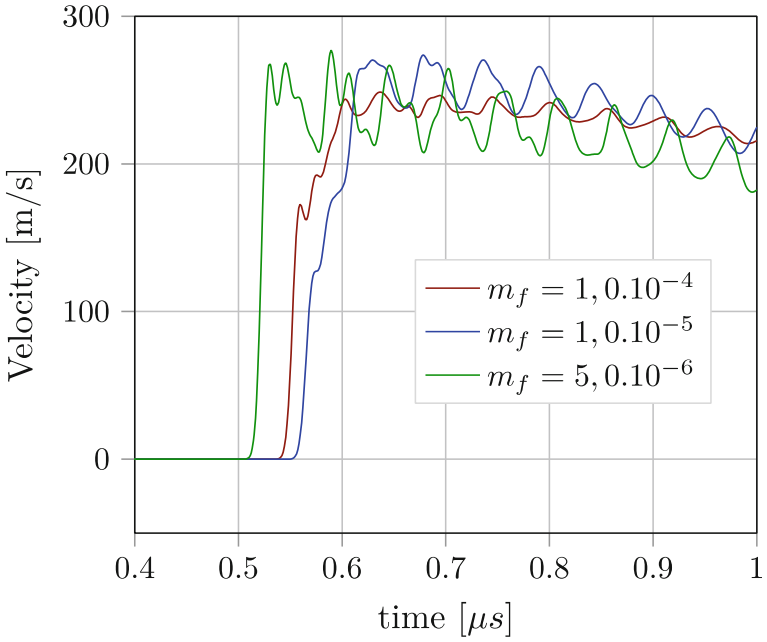

Fig. 2.15 Influence of the mesh size on the back face velocity

The velocity of the back obtained numerically is strongly sensitive to the interfacial stiffness of the model (Table 2.5). In order to evaluate this sensitivity, a parametric study is proposed. Figure 2.9 shows the sensitivity of the free surface velocity to the interfacial stiffness parameter K. Rather small discrepancies occur after 0.8 µs which is already far from the period of interest when delamination is initiated. Higher interfacial stiffness results in a drop of the free surface velocity, which means a reduction of the free surface bulging, due to a higher bending moment (Fig. 2.17).

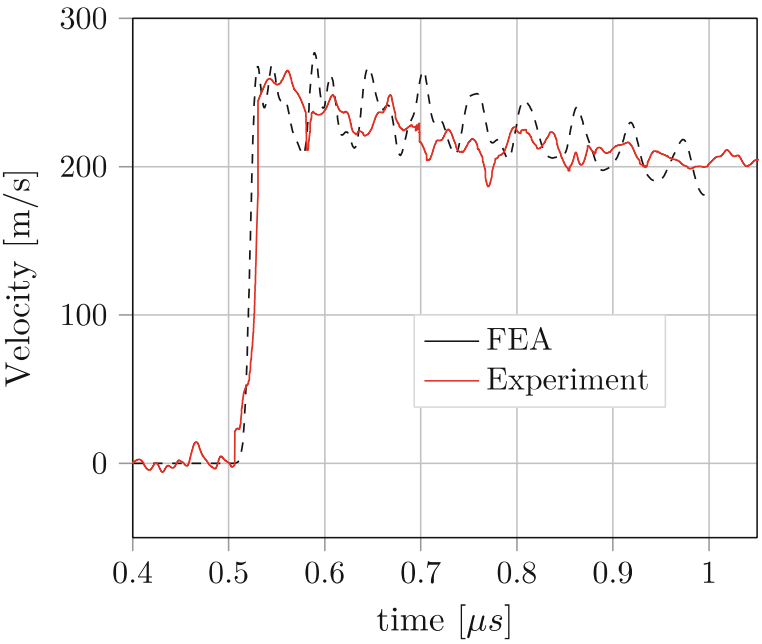

Fig. 2.16 Comparison of numerical and experimental velocity

Fig. 2.17 Influence of the interfacial stiffness on the back face velocity

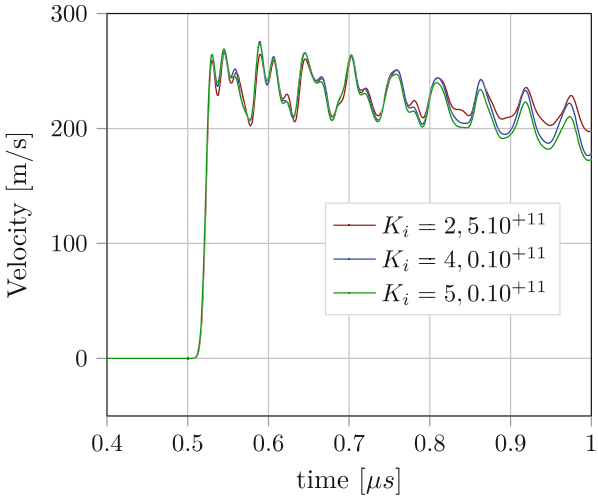

2.5 Conclusion

In this study, a promising technique, derivate from the Laser Shock Adhesion Test, was successfully experienced to delaminate at very high strain rate a Ultra High Molecular Weight PolyEthylene composite material that is commonly used for the development of light weight armors and of ballistic protection. It was assessed that the technique is able to generate pressure loading comparable to those exerted by a ballistic impact. The duration of the laser induced shock loading is however of the order of thousand times shorter than the one of a ballistic impact. This allows tests at the laboratory scale and also its use for reduced scale samples, which presents economic interest. In addition, a spatial shape of the laser induced shock has been determined. It remains a key parameter as input data in the Finite Element Model. The numerical simulation, based on contact cohesive interactions in Finite Element Methods, has brought major advances in the modelling of the delamination. They provided a good agreement with Photonic Doppler Velocimetry records. The influence of the interfacial stiffness parameter has been studied and it is observed that its best value is of $2.5.10^{+11}$ N. Larger values yielded to underestimate the bulging of the free surface when it is spalled. The numerical simulation of the delamination showed a multi delamination, suspected since observed in larger samples impacted by real bullets in [15] but not evidenced in thinner samples subjected to laser induced shock waves due to the difficulty of obtaining a clear cut and polishing of the recovered samples. This is an issue that could be extensively prospected by the future use of a high resolution microtomograph. In the future, the parameter G_i^c will also be the object of further research in order to be better estimated. At last, another outlook will be to subject various composite materials for ballistic protection to the laser delaminator in order to point out the most resilient ones with respect to the delamination process.

Acknowledgements Authors would like to thanks NATO for having granted the "Soft target protection" workshop SPS ARW G5524. Authors also thanks the European Commission for allowing Luminita ALIL's mobility in the frame of the ERASMUS program. At last, Authors thanks Region Bretagne, Finistère and Brest Métropôle Océane for their financial supports.

References

1. Chen X (ed) (2016) Advanced fibrous composite materials for ballistic protection. Woodhead Publishing, Oxford
2. Bhatnagar A (ed) (2016) Lightweight ballistic composites: military and law-enforcement applications. In: Woodhead publishing, San Diego
3. Cunniff PM, Auerbach MA, Vetter E, Sikkema DJ (2002) High performance "M5" fiber for ballistics/structural composites. In: 23rd. Army science conference, pp 1–8
4. Zhang D, Sun Y, Chen L, Zhang S, Pan N (2014) Influence of fabric structure and thickness on the ballistic impact behavior of ultra high molecular weight polyethylene composite laminate. Mater Des 54:315–322

5. Lässig T, Bagusat F, Pfändler S, Gulde M, Heunoske D, Osterholz J, May M (2017) Investigations on the spall and delamination behavior of UHMWPE composites. Compos Struct 182:590–597
6. Hopkinson B (1914) A method of measuring the pressure produced in the detonation of high explosives or by the impact of bullets. Philos Trans R Soc London, Ser A 213 (497–508):437–456
7. Hutchings IM (1983) The behaviour of metals under ballistic impact at sub-ordnance velocities. In: Material behavior under high stress and ultrahigh loading rates. Springer, Boston, pp 161–196
8. Tham CY, Tan VBC, Lee HP (2008) Ballistic impact of a KEVLAR® helmet: experiment and simulations. Int J Impact Eng 35(5):304–318
9. Fabbro R, Peyre P, Berthe L, Scherpereel X (1998) Physics and applications of laser-shock processing. J Laser Appl 10(6):265–279
10. Bolis C, Berthe L, Boustie M, Arrigoni M, Barradas S, Jeandin M (2007) Physical approach to adhesion testing using laser-driven shock waves. J Phys D Appl Phys 40(10):3155
11. Berthe L, Fabbro R, Peyre P, Tollier L, Bartnicki E (1997) Shock waves from a water-confined laser-generated plasma. J Appl Phys 82(6):2826–2832
12. Gay E, Berthe L, Boustie M, Arrigoni M, Trombini M (2014) Study of the response of CFRP composite laminates to a laser-induced shock. Compos Part B 64:108–115
13. Alil LC, Arrigoni M, Badea SM, Barbu C, Istrate M, Mostovykh PS (2017) On the constitutive law for the mechanical quasi-static response of criss-cross composites (on the example of UHMWPE). Hum Factors Mech Eng Def Safety 1(1):4
14. Matache LC, Alil LC, Rotariu T, Sandu SM, Puica C, Barbu C, Zecheru T (2018) Numerical validation of a constitutive model for Uhmwpe-based composites at high strain rates. Politeh Univ Buchar Sci Bull Ser B Chem Mater Sci 80(3):229–246
15. Alil LC, Arrigoni M, Badea S, Ginghină R, Matache LC, Mostovykh P (2018) Ballistic study of Tensylon®-based panels. Express Polym Lett 12(6):491–504
16. Alil LC, Matache LC, Sandu SM (2018) Numerical simulation of a ballistic impact on Tensylon UHMWPE laminates using the plastic kinematic model in LS-dyna. J Military Technol 1:n°1
17. Alil LC, Arrigoni M, Deleanu L, Istrate M (2018) Assessment of delamination in Tensylon® UHMWPE composites by laser-induced shock. Mater Plast 55(3):364
18. Prudhomme G, Mercier P, Berthe L, Bénier J, Frugier PA (2014) Frontal and tilted PDV probes for measuring velocity history of laser-shock induced calibrated particles. J Phys Conf Ser 500 (14):142022
19. Novikov SA, Divnov II, Ivanov AG (1966) The study of fracture of steel, aluminum, and copper under explosive loading. Phys Metals Metal Sci (USSR) 21(4):608–615
20. Bourguille J, Bergamasco L, Tahan G, Fuster D, Arrigoni M (2017) Shock propagation effects in multilayer assembly including a liquid phase. In: Key engineering materials, vol 755. Trans Tech Publications, Pfaffikon, pp 181–189
21. Bardy S, Aubert B, Berthe L, Combis P, Hébert D, Lescoute E, Videau L (2016) Numerical study of laser ablation on aluminum for shock-wave applications: development of a suitable model by comparison with recent experiments. Opt Eng 56(1):011014
22. Tahan G (2018) Etude des assemblages collés sous choc et de leurs propriétés mécaniques après choc laser, PhD thesis, ENSTA Bretagne, 13th of December 2018 (in French)
23. Žmindák M, Pelagić Z, Pastorek P, Močilan M, Vybošťok M (2016) Finite element modelling of high velocity impact on plate structures. Procedia Eng 136:162–168